

# REVEALING THE ABRASION RESISTANCE OF META-STABLE TITANIUM ALLOYS USING MULTI-PASS DUAL-INDENTER TESTS

## UGOTAVLJANJE ABRAZIJSKE ODPORNOSTI METASTABILNIH TITANOVIH ZLITIN Z UPORABO KOMBINIRANIH PREIZKUSOV RAZENJA IN INDENTACIJE

Hui Xiao<sup>1</sup>, Can Huang<sup>2</sup>, Jian Chen<sup>2</sup>, Cong Li<sup>2\*</sup>

<sup>1</sup>School of Mechatronics Engineering and Automation, Foshan University, Foshan 528001, China

<sup>2</sup>School of Energy and Power Engineering, Changsha University of Science and Technology, Changsha, Hunan 410114, China

*Prejem rokopisa – received: 2020-06-10; sprejem za objavo – accepted for publication: 2021-03-15*

doi:10.17222/mit.2020.018

The abrasion resistance of the Ti-5Al-4Zr-4Mo-2Cr-2Sn-1Fe alloy was investigated using multi-pass dual-indenter (MPDI) scratch tests with different loading conditions under a repetitive local sliding contact. Various microstructures were obtained with different heat treatments. The effect of the phase morphology on the scratch resistance and corresponding failure mechanisms were revealed. Results show that the phase morphology has a great influence on the scratch resistance and that the effect is contact-load dependent. The scratch behaviour is linked to the initial surface hardness at low loading conditions, while the work-hardening ability is more relevant at high loading conditions.

Keywords: titanium alloy, abrasion resistance, scratch test, microstructure

Avtorji so z uporabo kombiniranega testerja razenja in indentacije (MPDI, angl.: Multi-pass-dual-indenter) ugotavljali abrazijsko odpornost zlitine Ti-5Al-4Zr-4Mo-2Cr-2Sn-1Fe pri različnih obremenitvah in ponavljajočem drsnem kontaktu. Z različnimi toplotnimi obdelavami izbrane zlitine so dobili različne mikrostrukture. Ugotavljali so vpliv morfologije faz na odpornost zlitine na razenje in odgovarjajoče mehanizme porušitve. Rezultati raziskave so pokazali, da ima velik vpliv na odpornost zlitine proti razenju njena morfologija faz, ta pa je odvisna od obremenitve kontakta. Obnašanje zlitine med razenjem je povezano z začetno trdoto zlitine pri manjših obremenitvah, medtem ko so za mehansko utrjevanje zlitine bolj pomembni pogoji pri višjih obremenitvah.

Keywords: zlitina na osnovi titana, odpornost proti abraziji, test razenja, mikrostruktura

## 1 INTRODUCTION

Combining high mechanical properties, low density and excellent corrosion resistance in the past decades, titanium alloys have been not only adopted as the standard materials for pipes, fittings, valves and similar equipment in the chemical-process industry, but are also widely used in aeronautical and biomedical applications.<sup>1-3</sup> Pieces of equipment made from titanium alloys do their job well from the mechanical and corrosion standpoints, but occasionally the alloys must be used in parts of equipment that involve sliding the titanium against other materials, creating a titanium tribosystem. However, titanium alloys, being extremely reactive metals, are known for their poor tribological properties, posing a major problem for their use in industrial machinery.<sup>4</sup>

Abrasion is a common wear mechanism, often observed in various industrial applications. The response of materials in a tribological system is complex. To meet the commercial demands for a combination of a high

abrasion resistance and low price, the abrasive wear behaviour of a large variety of titanium alloy grades has been studied in industry and at academic centres in order to deepen our understanding and tune the alloy grade to the targets set. Many investigations on this issue were carried out. H. Schmidt et al.<sup>5</sup> studied the compound formation and abrasion resistance of ion-implanted Ti-6Al-4V and found that ion implantation of carbon or nitrogen into Ti-6Al-4V leads to a pronounced reduction in the oxide-particle abrasion. The maximum abrasion resistance is achieved by combining a high microhardness of the implanted layer and a low oxide-film thickness on the surface. T. Sawase et al.<sup>6</sup> demonstrated that a TiN surface coating can improve the abrasion resistance of pure titanium. Y. Zhu et al.<sup>7</sup> confirmed that the deposition of a TiC film on titanium with ion-enhanced triode plasma CVD and a carbide layer formed on the surface of Ti due to heating in a hydrocarbon atmosphere can result in a high abrasion resistance. The mild-to-severe wear transition of two titanium alloys, Ti-10V-2Fe-3Al and Ti-6Al-4V, was investigated and the correlation between the microstructure and wear micromechanisms was also studied; it was revealed that the subsurface

\*Corresponding author's e-mail:  
liconghntu@126.com (Cong Li)

work-hardening layer plays a very important role in determining the abrasion-wear resistance.<sup>8</sup>

Scratch testing involves the sliding of a rigid indenter with a fixed shape along a smooth surface under controlled load and speed, simulating the wear process and evaluating the wear resistance of various materials. However, the traditional scratch test starts at a new undeformed surface, which may be very different from the surface formed in a wear process, so it cannot really reflect the wear-resistance response of materials.<sup>9,10</sup> In the actual abrasion process, using the conventional scratch test to predict the wear mechanism, will lead to serious errors and mislead people's understanding of the wear resistance.<sup>11</sup> However, in all the experimental scratch studies on titanium alloys, an original surface and a single indenter were used.<sup>12,13</sup>

In the current work, a new multi-pass dual-indenter scratch-test methodology developed by X. Xu et al.<sup>14, 15</sup> was employed to approach the real abrasion condition by carrying out scratch tests using a large indenter to generate a wide pre-scratch with stable saturated work hardening and a small indenter to evaluate the wear behaviour. This test method not only detects the damage formation during the actual scratching process but also probes its interaction with the damage in the deformed surface layer caused by prior local plastic deformations. A commercial metastable  $\beta$  titanium alloy, Ti-5Al-4Zr-4Mo-2Cr-2Sn-1Fe, (abbreviated as  $\beta$ -Cez) invented by the Cezus Company from France was selected for this research. In this alloy, the nominal  $\beta$ -transus temperature of the alloy is about  $(870 \pm 5)$  °C. The abrasion resistance of different microstructures was studied with the new scratch test under different pre-scratch conditions. The development of the worn scar and subsurface layer was studied. The damage mechanism under different test conditions was analysed.

## 2 EXPERIMENTAL PART

The chemical-composition analysis results of the target alloys are listed in **Table 1**. The initial microstructure of the alloy is shown in **Figure 1**. It can be seen that the matrix of the alloy is mainly composed of fine equiaxed  $\alpha$  (a grain size of 7  $\mu$ m), short rod-like  $\alpha$  phase and  $\beta$  phase. This is a typical bi-modal structure. Rectangular samples of 10 mm in length, 6 mm in width and a thickness of 4 mm were machined from a thick as-received slab using electrical discharge machining (EDM). Prior to further experiments, the thin oxide layer was removed with careful mechanical polishing. The samples were heat-treated in a NABERTHERM furnace, filled with argon at different temperatures, and then quenched to room temperature with water. **Table 2** lists the details of heat-treatment conditions. For further experiments, the samples were installed in a cold setting resin and polished according to the standard metallographic preparation. Different phases of the two alloys were unravelled with the standard Kroll reagent (3 mL HF + 6 mL HNO<sub>3</sub>

+ 100 mL H<sub>2</sub>O). The microstructure was determined with a Leica LF7M38 optical microscope.

A linear reciprocating ball-on-block wear test was performed using a tribometer (UTM-3, USA) with a  $\phi$ 3 mm hardened chrome steel ball (100 Cr6, 58-63 HRC) as the counterpart. The top surfaces of the specimens were ground using a series of SiC grinding papers with various sizes up to 2000 grit. The specimens were then polished on a velvet cloth using a series of Al<sub>2</sub>O<sub>3</sub> powder (up to 1  $\mu$ m) suspended in distilled water. Just before testing, all the specimens were ultrasonically cleaned in an alcohol bath for 15 min. All the tests were performed with a 5-N constant load, 10-mm linear oscillatory motion, 240-mm·min<sup>-1</sup> speed and 40-min loading duration. The characteristic morphologies of the worn surfaces were analysed with a three-dimensional super-depth-of-field microscope (VHX1000, Japan).

**Table 1:** Composition analysis of the target alloy (w%)

Alloy	Al	Zr	Mo	Cr	Sn	Fe	Ti
$\beta$ -Cez	5.02	4.25	3.90	1.9	2.1	0.91	Balance

**Table 2:** Performed heat treatments of  $\beta$ -Cez alloy

$\alpha + \beta$ solution treatments	800 °C / 30 min
$\beta$ solution treatments	950 °C / 15 min
$\beta + (\alpha + \beta)$ solution treatments	950 °C / 15 min + 750 °C / 15 min
$\beta$ solution + aging	950 °C / 15 min + Q + 550 °C / 15 min

Scratch tests were performed using a CSM micro-scratch tester. Two spherical diamond Rockwell indenters with different tip radius and cone angles were employed in the current study: a large indenter (J-191) with a tip radius of 100  $\mu$ m and a cone angle of 120° and a small indenter (SM-A15) with a tip radius of 5  $\mu$ m and a cone angle of 60°. Two testing modes were employed in the conditions specified in **Table 3**.

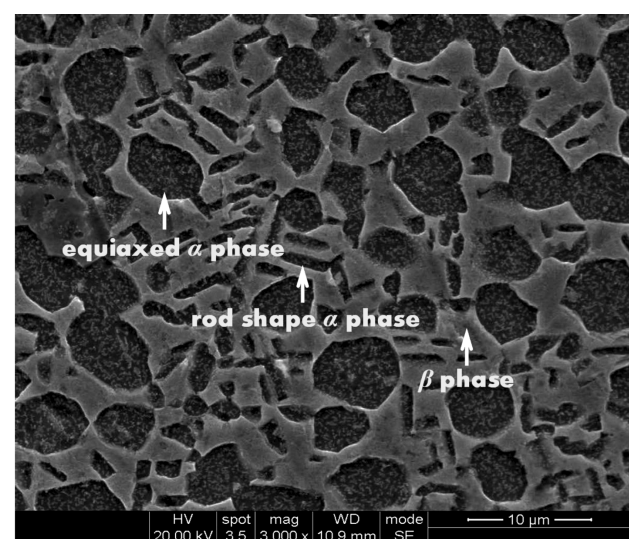


**Figure 1:** As-received microstructure of the alloy

**Table 3:** Test conditions of different scratch modes

Scratch modes	Test conditions of the large indenter	Test conditions of the small indenter
Mode 1	NA	Single pass with constant load of 0.3 N
Mode 2	Multi-pass with (5, 10, 15, 20, 25) N	Single pass with constant load of 0.3 N

For the Mode 1 testing, the small indenter slides directly on the initial (polished) surface. For the Mode 2 (MPDI) testing, the small indenter slides over the centre of a 2 mm long pre-scratch, produced by sliding the large indenter 10 times (always in the same direction) over the surface under different loads. The sliding speeds of the large and small indenter were 0.2 mm/s and 0.05 mm/s, respectively. All the sliding tests were conducted in the same direction. Each test was repeated three times to make sure that reproducible behaviour was observed and reported. **Figure 2** shows a schematic drawing of the observations of the scratch track. The area enclosed by a blue dashed line refers to the pre-scratch track produced by the large indenter. The scratch track created by the small indenter is at the middle bottom of the big pre-scratch track corresponding to the zone marked by the red dashed line. The scratch depth to be plotted in

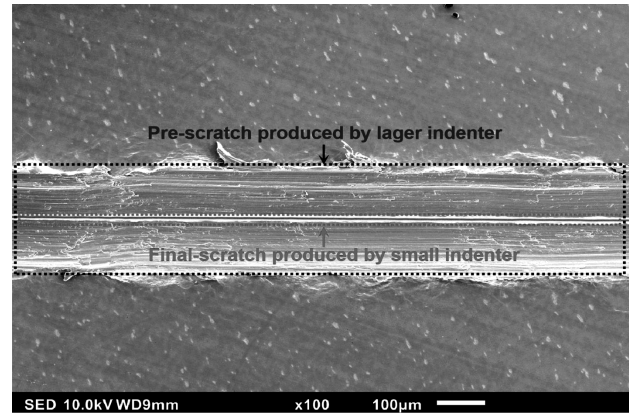


**Figure 2:** The schematic drawing of scratch tracks

this paper refers to the penetration depth of the small-indenter scratching with respect to the bottom of the wear track produced by the large indenter. After the scratch tests, the worn surface was observed with a high-resolution JEOL scanning electron microscope operating at 5 kV. Microhardness measurements on the pristine samples were carried out using a Vickers indenter and a load of 2 N, and making 10 independent measurements.

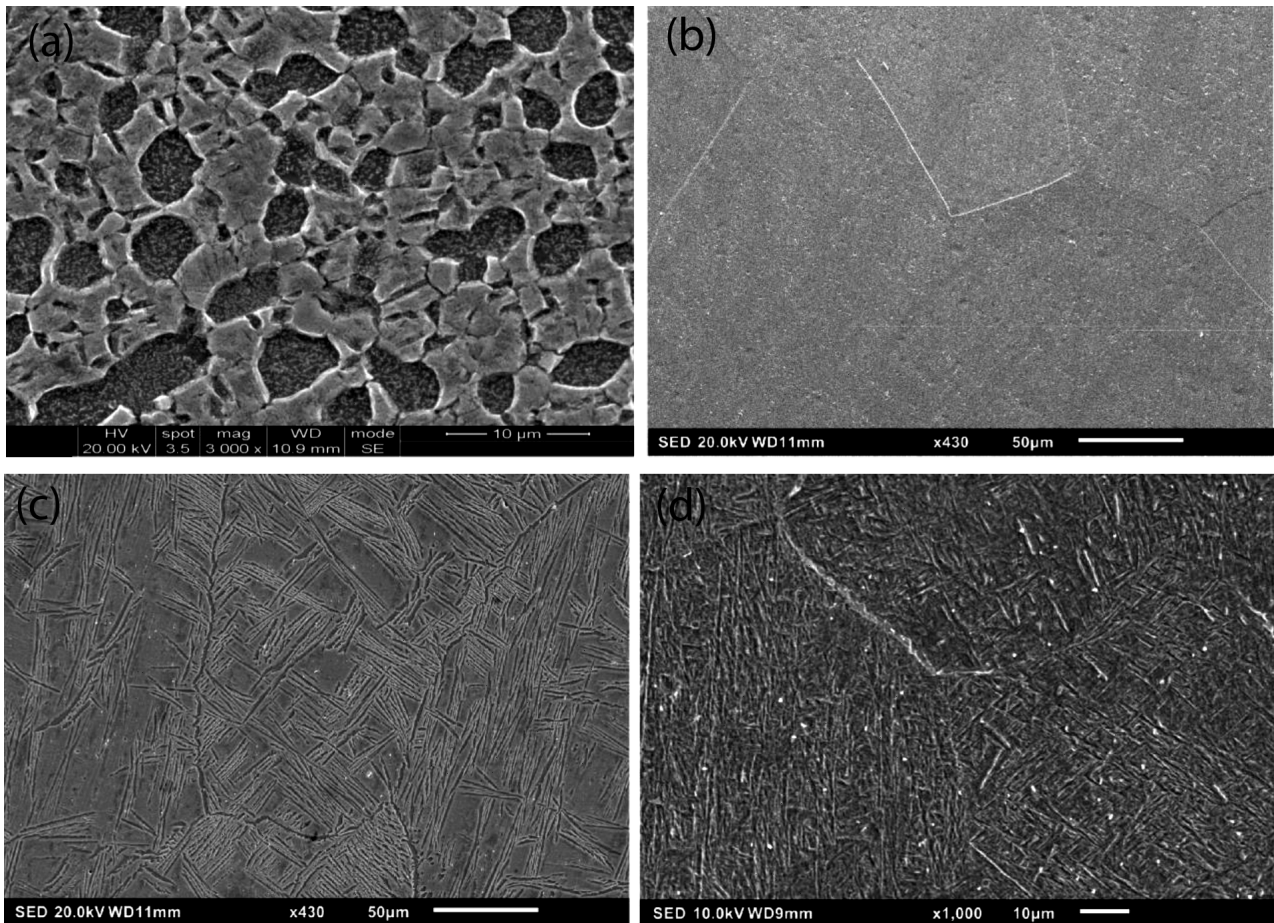


**Figure 3:** Different microstructure of Ti alloy with different heat treatment: a) 850 °C/30 min, b) 950 °C/15 min, c) 950 °C/15 min + 750 °C/15 min, d) 950 °C/15 min + Q + 550 °C/15 min

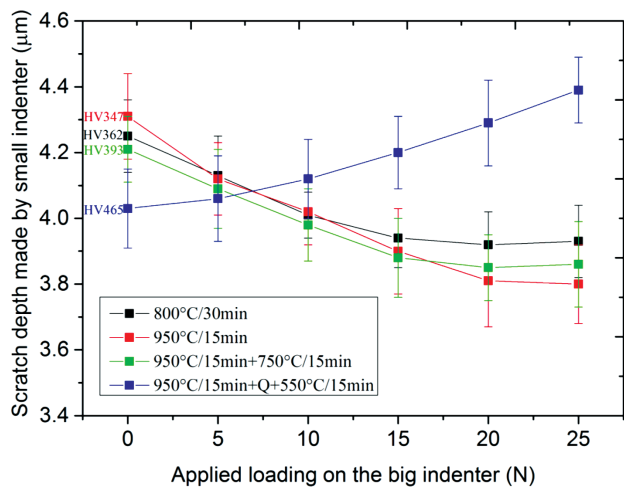


**Figure 4:** The scratch depth as a function of applied load on the large indenter

After heat treatments, cylindrical samples with a diameter of 4 mm and length of 7 mm were compressed at room temperature by a Gleeble 1500 machine. The strain rate was  $10^{-3} \text{ s}^{-1}$ . To ensure the accuracy and repeatability of the experimental results, each compression test was repeated three times.

### 3 RESULTS AND DISCUSSION

Different heat treatments result in different microstructures. Some samples were heat treated directly at 800 °C for 30 min, which was lower than the temperature of  $\beta$ -transus. The optical micrograph after the solution treatment is shown in **Figure 3a**. It can be seen that the microstructure of the sample is very similar to that of the initial state. The grain size of the  $\alpha$ -phase is about 5–10  $\mu\text{m}$ , which appears in different morphologies, such as globular shape and lath shape, embedded in the  $\beta$  matrix. Some of the samples were heat treated directly at 950 °C for 15 min, which was higher than the  $\beta$ -transus temperature. The microstructure is shown in **Figure 3b**. Specimens exhibit coarse  $\beta$  grains with a grain size of 200–400  $\mu\text{m}$ . The microstructure of the alloy is homogeneous without any other visible transformations. This in-

dicates that the  $\beta$  phase of this alloy is stable enough to keep the high-temperature  $\beta$  phase at room temperature. The  $\beta + (\alpha + \beta)$  treatment involves a  $\beta$  homogenization followed by cooling to the  $\alpha + \beta$  field before quenching to room temperature. After this heat treatment, the samples exhibit different features (**Figure 3c**). Intermediate annealing in the  $\alpha + \beta$  phase field results in a bulkier microstructure. Predominantly large retained prior  $\beta$  grains with a grain size of about 200–400  $\mu\text{m}$  along with a thick  $\alpha$  phase with different morphologies (laths and Widmanstätten) are obtained. The  $\alpha$ -Widmanstätten morphology is observed at the prior  $\beta$ -grain boundaries. The metallographic structure of the  $\beta$ -Cez alloy with annealing at a high temperature and aging at 550 °C for 15 min is shown in **Figure 3d**. It consists of large  $\beta$ -grains and very fine needle-like precipitates.

**Figure 4** shows the scratch depth due to the sliding with a sharp indenter as a function of the load applied on the large indenter. The microhardness values of each condition are also indicated. The scratch depth at the normal load 0 N corresponds to the penetration depth scratching on the original polished surface (Mode 1 test). For all the samples, there is a good consistency between the static hardness and the scratch depth of a 0 N data point. The scratch depth of the original surface is relatively high (the data points plotted as 0 N loads). For the alloy grades used for the solution treatment, the scratch depth first decreases with the increase in the loading of the large indenter. The decrease of the scratch depth reflects the surface hardening effect due to the pre-scratch. The trend of decreasing scratch depth with the increasing load on the large indenter continues up to the critical load, at which the scratch depth of the small indenter becomes unchanged. This scratch depth reflects the abrasive-material removal and interaction between the deformation field of the small indenter and the internal damage of the wear track. On the other hand, for aging samples, the depth of most scratches increases with the preload, indicating a decreasing abrasion resistance.

In order to clarify the relationship between the abrasion resistance and conventional mechanical properties, the heat-treated specimens were evaluated with compression tests and the conventional friction test. The stress-

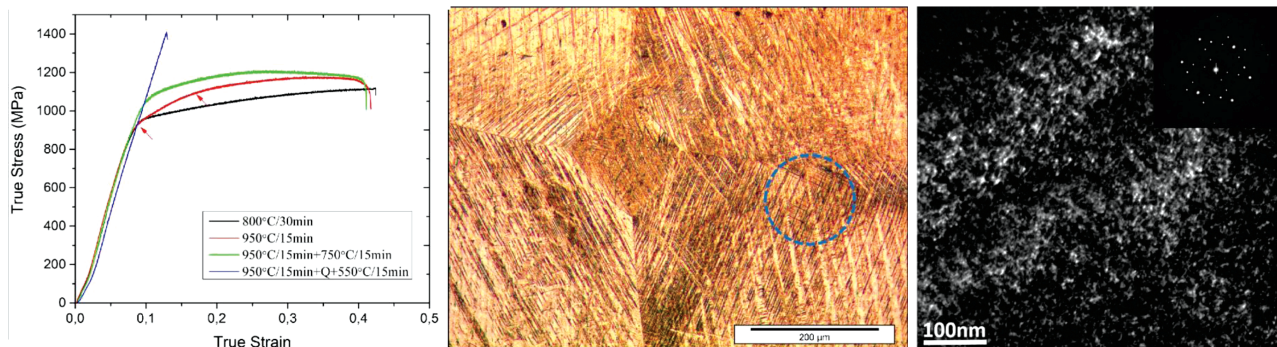


**Figure 5:** a) True stress-strain curves of different heat treated samples, b) the existence of SIM transformation, c) Dark field image and electronic diffraction of  $\omega$  phase

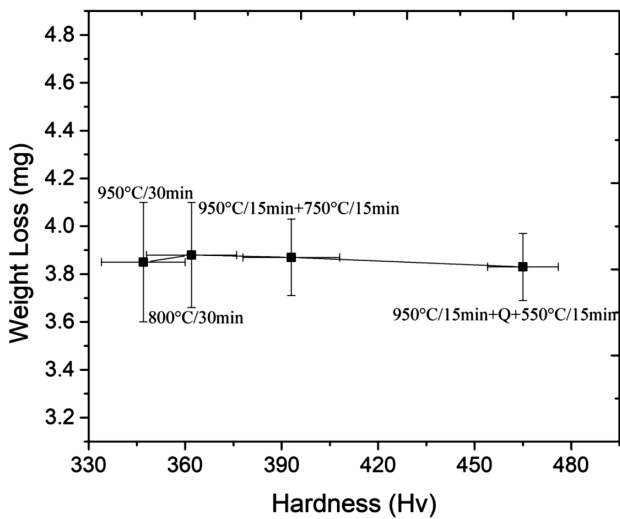


**Figure 6:** The weight loss as a function of hardness for four samples

strain curves are shown in **Figure 5a**. This figure shows that the solution-treated samples exhibit a slight difference in the mechanical properties, but the aging specimen presents a totally different curve. It is generally believed that the red curve with an obvious double yield point means that the stress-induced martensitic transformation occurs during deformation, and this kind of transformation can improve the balance of strength and plasticity, though also inevitably introducing a lower yield stress. The samples showing the SIM effect present a relatively high work-hardening rate, which is proved by the difference between the yield strength and ultimate compressive strength; the corresponding microstructure is shown in **Figure 5b**, as confirmed in our previous work.<sup>2</sup> It is worth noting that the scratch depth of the specimen with the stress-induced martensite (SIM) transformation effect decreases continuously with the increase of preloading. Unlike all the solution-treated samples shown previously, the quenched and aged samples did not show any macroscopic yield in any case. The existence of a very fine  $\omega$  phase (**Figure 5c**) with the ability

to resist dislocation movement is the main reason for the relatively high strength and low plasticity observed.

The average weight losses of the same samples in the wear tests plotted against the as-received initial hardness are shown in **Figure 6**. It is very interesting to note that regardless of the considerable differences in the initial hardness, the four grade alloys show a relatively small variation in the weight loss and there is no monotonous relation between the wear resistance and the initial hardness. Furthermore, as can be seen in this figure, the quenched and aged samples, which possess the highest initial hardness, display a wear resistance comparable to the other, much softer alloys. The order of abrasion resistance of the four alloys agrees with the order produced using the MPDI scratch test under the low pre-load conditions (especially for 5 N and 10 N).

**Figure 7** displays typical scratch grooves made by the small indenter on the pre-scratch track via the large indenter for the alloy heat treated at 950 °C / 15 min (SIM) and 900 °C / 15 min + Q + 550 °C / 15 min (NO SIM). Typical scratch grooves of the samples with a SIM effect are shown in **Figure 7a**. Due to a good combination of plasticity, strain hardening and strength, the scratch track is smooth without any delamination or crack. The scratch track of the aged sample shows that the failure mechanism is mainly ploughing, but there is some debris formation on the edge of the scratch because of the brittle nature and low work-hardening capability of the sample.

**Figure 8** shows the surface state of the samples after the traditional friction test. It can be seen from the figure that after different heat treatments, the worn surfaces of the materials after exposure to the friction test show a high degree of similarity and evidence of the same ploughing mechanism. It may be that the experimental load or time is not sufficient, so the anti-wear performance of various products is not fully reflected. Some small grooves produced during the experiments can be seen. A significant wear loss in the real process is a result of repeated interactions of multiple asperities, i.e., the sum of wear losses produced by different particles.

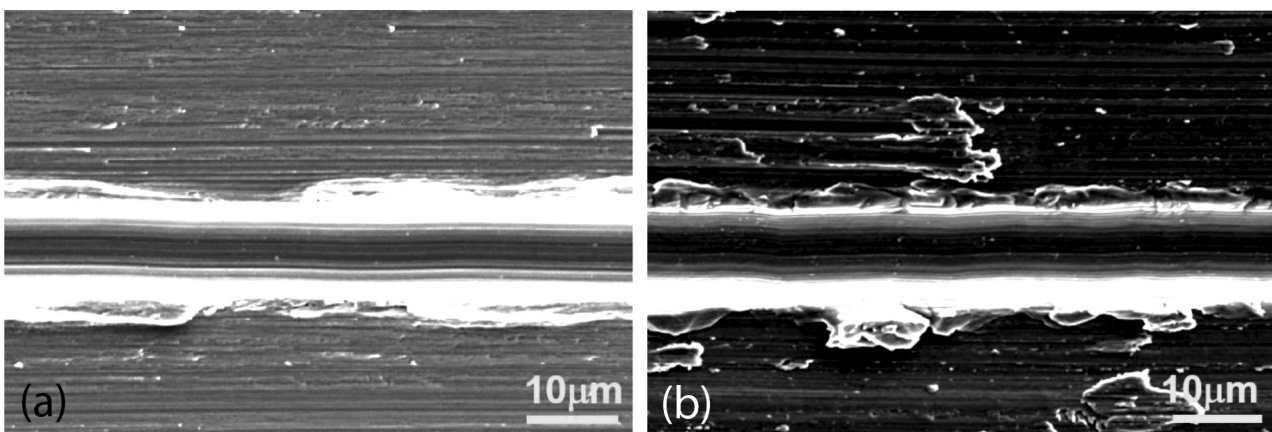


**Figure 7:** Typical scratch grooves made by the small indenter: a) 950 °C/15 min, b) 950 °C/15 min + Q + 550 °C/15 min

This result is in good agreement with the weight-loss curve from **Figure 6**. It should be noted that the quenched and aged sample has the highest hardness, but from the results for the worn surface, it is not significantly different from the other three samples. This confirms the experimental results for the MPDI under the

5-N and 10-N loads. It also shows that the MPDI test can reflect the wear resistance of an alloy under different loads.

In order to clarify the response of the material, microstructures of the cross-sections perpendicular to the scratch track were investigated with SEM. Typical re-

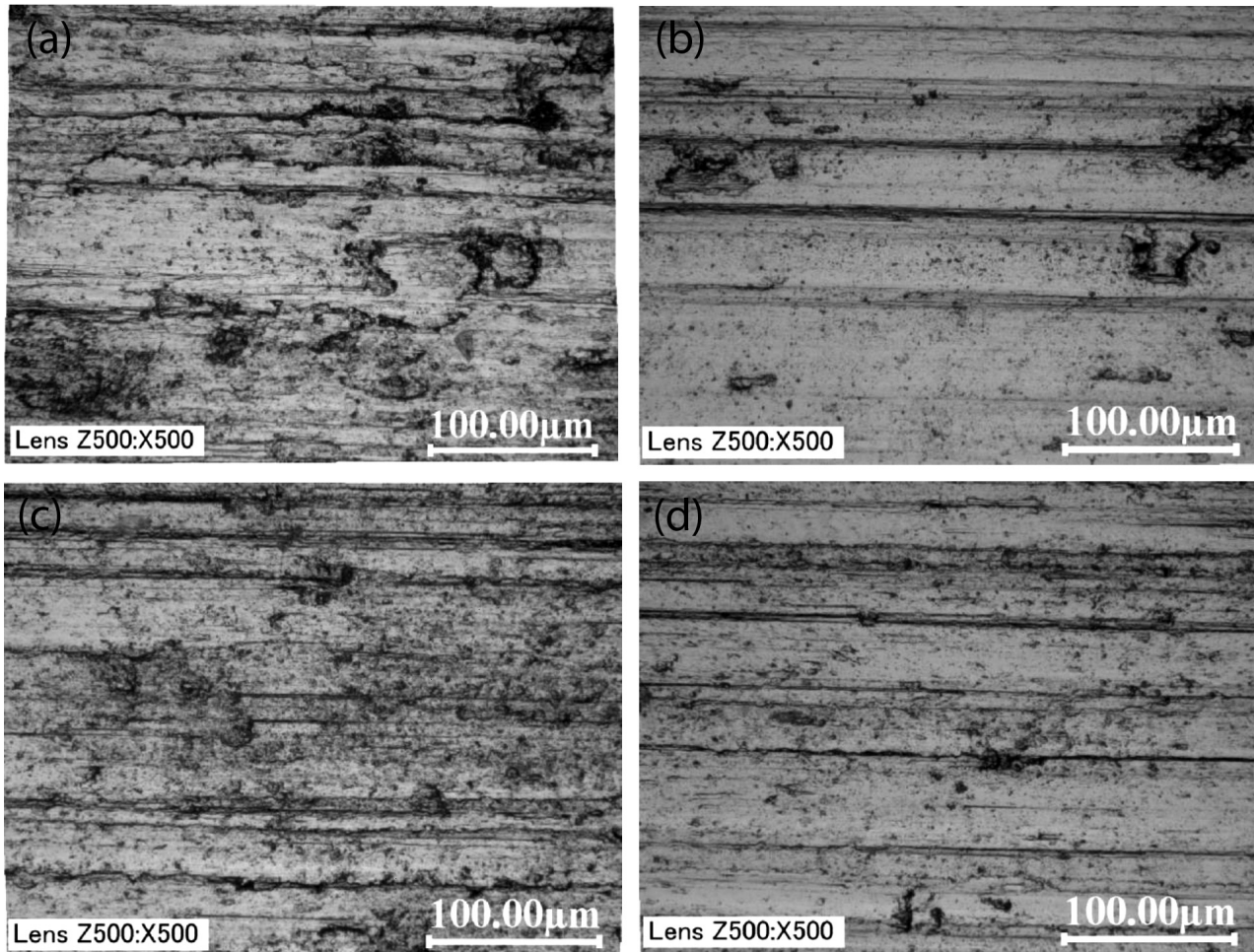


**Figure 8:** Different worn surface of Ti alloy with different heat treatment: a) 850 °C/30 min, b) 950 °C/15 min, c) 950 °C/15 min + 750 °C/15 min, d) 950 °C/15 min + Q + 550 °C/15 min

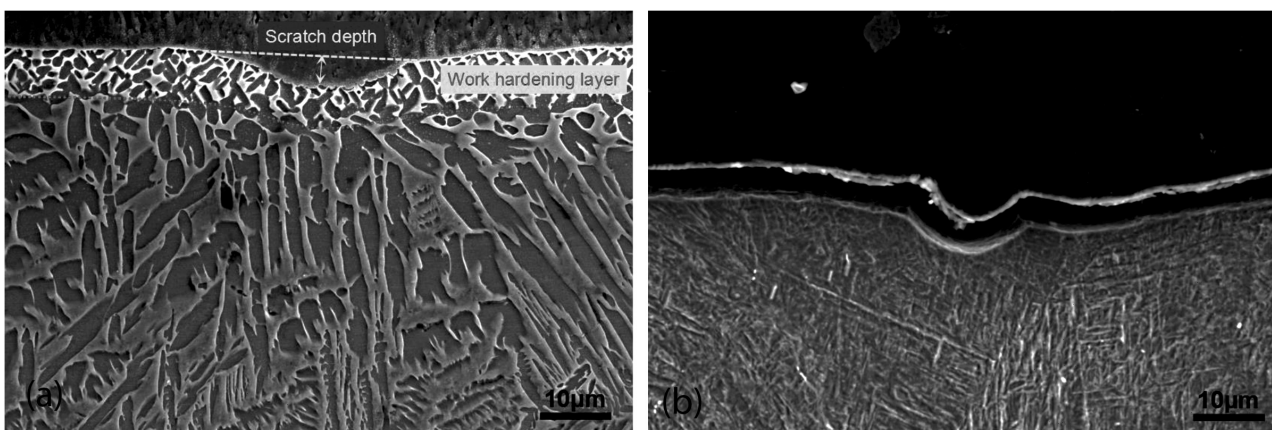


**Figure 9:** Microstructures of the cross-sections perpendicular to the scratch track: a) 950 °C/15 min + 750 °C/15 min, b) 950 °C/15 min + Q + 550 °C/15 min

sults are shown in **Figure 9**. The scratch created by the small indenter is indicated with a yellow-arrow line, while the boundaries of the work-hardening layer generated by the large indenter is marked with red dashed lines. It can be clearly seen that the samples after a solution treatment present an evident work-hardening layer. The microstructure of the subsurface is strongly changed by the pre-scratch, and shear deformation is inevitably introduced into the material, while the samples after an aging treatment barely show any hardening structure. According to our previous studies,<sup>2</sup> a large number of isothermal  $\omega$  phases are formed in the samples upon aging and this kind of phase is very hard and brittle. The figure also shows that the scratch of the small indenter is right in the area of the pre-scratch track, indicating that the scratch depth produced by the small indenter truly reflects the behaviour of the work-hardening layer.

During a real-life abrasion, abrasive particles continuously move along the surface, being strain hardened and abraded under local contact conditions. When a material undergoes abrasion, the top surface deforms severely and may result in different local failure modes, depending on the working condition, while the subsurface layer also responds to the external strain/stress and can be strain hardened to different degrees, depending on the microstructure and its strain-hardening capability. A severe deformation leads to a significant subsurface refinement and the thickness of such a layer also varies. As a consequence, the state of the abraded (subsurface) microstructures is quite different from the original state.

The scratch test, using a single rigid indenter of a controlled shape under a controlled load and speed against a smooth surface, mimicking the abrasion process, was shown to be a useful tool for evaluating the abrasion resistance of various microstructures. However, the conventional scratch tests are mostly done on the initial surface, which can be very different from those that form during an abrasion process, e.g., irregularity, continuous development of subsurface deformation and work hardening, etc.; hence, they do not automatically truly reflect the material abrasion-resistance response. Single-pass scratching of a pristine surface is an oversimplification of the actual situation, wherein new particles scratch the worn surface that underwent previous processes. To better simulate a real process, methodologies of multiple parallel scratching were proposed to include the interactions between scratches. Compared to a single-pass scratch on a pristine initial surface, all multiple-scratching methods provide more insight into the wear mechanisms, interactions of scratches and effects of work hardening.

Nevertheless, in all experimental set-ups reported to date, only one indenter was utilized and the new scratch was fully or partially superimposed on the previous scratch, which inevitably combined the effects of surface work hardening and contact geometry. Moreover, even

for the work hardening itself, after only one pre-scratch, the surface and subsurface layer may not reach a stable condition with saturated work hardening, which is most likely the case in a real continuous wear process. In order to mimic a real-life abrasion process and exclude the contact geometry effect, in this study, a new multi-pass dual-indenter scratch-test methodology is employed to create a real abrasion condition by carrying out scratch tests using a large indenter to generate a wide pre-scratch track (wear track) with stable, saturated work hardening, representing the subsurface layer formed during the real-life abrasion, and a small indenter sliding over the pre-scratched surface to evaluate the wear resistance and record the failure mechanism. Given that the purpose of the MPDI scratch test is to reveal the material response and associated failure mechanisms, without producing a wear loss in a continuous process, the MPDI scratch methodology only applies one extra scratch but under different preloading conditions.

Generally, the current method reflects the scratches on the work-hardening surface layer, which is more similar to the wear surface formed in a continuous wear process. By studying the effect of the load applied in the process of pre-scratching, the abrasion resistance under mild and heavy loads can be predicted. The results of the scratch test and microstructure study show that the scratch / wear resistance of the material depends not only on the initial hardness and microstructure of the material, but also on its deformation and work-hardening behaviour so that the failure mechanism of the material changes from one to another.

Several distinct microstructures were created with different heat-treatment processes: a near-spherical  $\alpha$  phase was produced with the solid-solution treatment in the two-phase region, metastable  $\beta$  grains were obtained when the annealing was done at a temperature well within the  $\beta$ -phase field, a flake  $\alpha$  phase or Widmanstätten  $\alpha$  phase was produced with the  $\beta + (\alpha + \beta)$  solid-solution treatment, a fine acicular  $\alpha$  phase and a high density of the  $\omega$ -nanophase formed when a high-temperature aging treatment was applied. For the solution-treated specimens, with the increasing load on the large indenter used to create a controlled wear track, the work hardening of the sub-surface led to a decrease in the scratch depth. However, if the  $\beta$  phase present is metastable, the stress-induced martensitic transformation of the samples with a low initial surface hardness leads to an enhancement of the surface hardening effect and a more obvious decrement of the scratch depth, i.e., a better abrasion resistance. Due to the ageing of the alloys, the formation of hard but brittle  $\omega$ -nanophase precipitates provides for an excellent wear resistance at low pre-loads, but with an increase in the load, its performance deteriorates. Because of the low work-hardening capacity, the improvement in the scratch resistance due to strain hardening is very limited or even absent. This phenomenon is well reflected in the MPDI test.

#### 4 CONCLUSIONS

In the current paper, a novel multi-pass dual-indenter scratch-test technology, originally developed to measure the abrasion resistance of steels, is applied here to study the abrasion resistance of the  $\beta$ -Cez alloy with different microstructures. It shows that the scratch behaviour is linked to the work-hardening ability, especially at high loading conditions, and that the initial surface hardness is more relevant at low loading conditions. The solution-treatment results including globular  $\alpha$ , flake  $\alpha$  or ductile metastable  $\beta$  can be better options for improving the abrasion resistance, instead of pursuing a microstructure with the highest static hardness via an ageing treatment. In this titanium alloy, the stress-induced martensite formation of the metastable  $\beta$  can significantly improve the abrasion resistance under high loads.

#### Acknowledgment

The authors gratefully acknowledge the financial support provided by the National Natural Science Foundation of China (Grant Nos. 51775055, 51975061), Natural Science Foundation of the Hunan Province (Grant Nos. 2018JJ3539, 2019JJ40300), Research Foundation of Education Bureau of the Hunan Province (Grant No. 19B033), China Postdoctoral Science Foundation (No. 2018M642973) and State Key Laboratory of Advanced Design and Manufacturing for Vehicle Body at the Hunan University (No. 31875004).

#### 6 REFERENCES

- <sup>1</sup> W. Chen, A. Yan, C. Wang, Y. Deng, D. C. Chen, H. Xiao, D. Zhang, X. Meng, Microstructures and mechanical properties of AlCrN/TiSiN nanomultilayer coatings consisting of fcc single-phase solid solution, *Applied Surface Science*, 509 (2020), 145303, doi:10.1016/j.apsusc.2020.145303
- <sup>2</sup> C. Li, L. Qin, M. Li, H. Xiao, Q. Wang, J. Chen, Influence of deformation strain rate on the mechanical response in a metastable  $\beta$  titanium alloy with various microstructures, *Journal of Alloys and Compounds*, 815 (2020), 152426, doi:10.1016/j.jallcom.2019.152426
- <sup>3</sup> W. Chen, T. Hu, C. Wang, H. Xiao, X. Meng, The effect of microstructure on corrosion behavior of a novel AlCrTiSiN ceramic coating, *Ceramics International*, 46 (2020), 12584–12592, doi:10.1016/j.ceramint.2020.02.022
- <sup>4</sup> C. Li, M. Li, H. Li, J. Chen, H. Xiao, Influence of solution treatment on microstructural evolution and mechanical properties of a new titanium alloy, *Kovove Materijali*, 58 (2020), 41–48, doi:10.4149/km\_2020\_1\_41
- <sup>5</sup> H. Schimdt, A. Schminke, M. Schmiedgen, B. Baretzky, Compound formation and abrasion resistance of ion-implanted Ti6Al4V, *Acta Materialia*, 49 (2001), 487–495, doi:10.1016/S1359-6454(00)00326-8
- <sup>6</sup> T. Sawase, K. Yoshida, Y. Taira, K. Kamada, M. Atsuta, K. Baba, Abrasion resistance of titanium nitride coatings formed on titanium by ion-beam-assisted deposition, *Journal of Oral Rehabilitation*, 32 (2005), 151–157, doi:10.1111/j.1365-2842.2004.01382.x
- <sup>7</sup> Y. Zhu, W. Wang, X. Jia, T. Akasaka, S. Liao, F. Watari, Deposition of TiC film on titanium for abrasion resistance implant material by ion-enhanced triode plasma CVD, *Applied Surface Science*, 262 (2012), 156–158, doi:10.1016/j.apsusc.2012.03.152
- <sup>8</sup> K. Farokhzadeh, A. Edrissy, Transition between mild and severe wear in titanium alloys, *Tribology International*, 94 (2016), 98–111, doi:10.1016/j.triboint.2015.08.020
- <sup>9</sup> G. Subhash, W. Zhang, Investigation of the overall friction coefficient in single-pass scratch test, *Wear*, 252 (2002), 123–134, doi:10.1016/S0043-1648(01)00852-3
- <sup>10</sup> A. Vencl, N. Manic, V. Popovic, M. Mrdak, Possibility of the abrasive wear resistance determination with scratch tester, *Tribology Letters*, 37 (2010), 591–604, doi:10.1007/s11249-009-9556-x
- <sup>11</sup> X. Xu, S. van der Zwaag, W. Xu, Prediction of the abrasion resistance of construction steel on the basis of the subsurface deformation layer in a multi-pass dual-indenter scratch test, *Wear*, 338–339 (2015), 47–53, doi:10.1016/j.wear.2015.05.012
- <sup>12</sup> I. P. Semenova, R. R. Valiev, K. S. Selivanov, Y. M. Modina, A. V. Polyakov, M. K. Smyslova, R. Z. Valiev, Enhanced strength and scratch resistance of ultra-fine grained Ti64 alloy with (Ti+V)N coating, *Review of Advanced Materials Science*, 48 (2017), 62–70, [http://www.ipme.ru/e-journals/RAMS/no\\_14817/05\\_14817\\_valiev.pdf](http://www.ipme.ru/e-journals/RAMS/no_14817/05_14817_valiev.pdf)
- <sup>13</sup> K. Holmberg, A. Laukkanen, H. Ronkainen, J. Li, W. Beres, Three-dimensional finite element modelling of the scratch test for a TiN coated titanium alloy substrate, *Wear*, 260 (2006), 1232–1242, doi:10.1016/j.wear.2005.08.008
- <sup>14</sup> X. Xu, S. van der Zwaag, W. Xu, A novel multi-pass dual-indenter scratch test to unravel abrasion damage formation in construction steels, *Wear*, 322–323 (2015), 51–60, doi:10.1016/j.wear.2014.10.011
- <sup>15</sup> C. Li, H. Li, S. van der Zwaag, Unravelling the abrasion resistance of two novel meta-stable titanium alloys on the basis of multi-pass-dual-indenter test, *Wear*, 400–441 (2019), 203094, doi:10.1016/j.wear.2019.203094